Metabolic Engineering 59 (2020) 64–75

Contents lists available at ScienceDirect

Metabolic Engineering

journal homepage: www.elsevier.com/locate/meteng

Engineering glucose metabolism for enhanced muconic acid production in *Pseudomonas putida* KT2440

Gayle J. Bentley[a], Niju Narayanan[b], Ramesh K. Jha[b], Davinia Salvachúa[a], Joshua R. Elmore[c,d], George L. Peabody[c], Brenna A. Black[a], Kelsey Ramirez[a], Annette De Capite[a], William E. Michener[a], Allison Z. Werner[a], Dawn M. Klingeman[c], Heidi S. Schindel[c], Robert Nelson[a], Lindsey Foust[a], Adam M. Guss[c], Taraka Dale[b], Christopher W. Johnson[a,**], Gregg T. Beckham[a,*]

[a] National Bioenergy Center, National Renewable Energy Laboratory, Golden, CO, 80401, USA
[b] Bioscience Division, MS M888, Los Alamos National Laboratory, Los Alamos, NM, 87545, USA
[c] Biosciences Division, Oak Ridge National Laboratory, Oak Ridge, TN, 37831, USA
[d] Current Address: Biosciences Division, Pacific Northwest National Laboratory, Richland, WA, 99354, USA

ARTICLE INFO

Keywords:
cis,cis-muconic acid
Pseudomonas putida KT2440
Glycolysis regulation
HexR
2-Ketogluconate
Gluconate
GacS
Biosensor
Adaptive laboratory evolution
CatM
FACS
High throughput selection

ABSTRACT

Pseudomonas putida KT2440 has received increasing attention as an important biocatalyst for the conversion of diverse carbon sources to multiple products, including the olefinic diacid, *cis,cis*-muconic acid (muconate). *P. putida* has been previously engineered to produce muconate from glucose; however, periplasmic oxidation of glucose causes substantial 2-ketogluconate accumulation, reducing product yield and selectivity. Deletion of the glucose dehydrogenase gene (*gcd*) prevents 2-ketogluconate accumulation, but dramatically slows growth and muconate production. In this work, we employed adaptive laboratory evolution to improve muconate production in strains incapable of producing 2-ketogluconate. Growth-based selection improved growth, but reduced muconate titer. A new muconate-responsive biosensor was therefore developed to enable muconate-based screening using fluorescence activated cell sorting. Sorted clones demonstrated both improved growth and muconate production. Mutations identified by whole genome resequencing of these isolates indicated that glucose metabolism may be dysregulated in strains lacking *gcd*. Using this information, we used targeted engineering to recapitulate improvements achieved by evolution. Deletion of the transcriptional repressor gene *hexR* improved strain growth and increased the muconate production rate, and the impact of this deletion was investigated using transcriptomics. The genes *gntZ* and *gacS* were also disrupted in several evolved clones, and deletion of these genes further improved strain growth and muconate production. Together, these targets provide a suite of modifications that improve glucose conversion to muconate by *P. putida* in the context of *gcd* deletion. Prior to this work, our engineered strain lacking *gcd* generated 7.0 g/L muconate at a productivity of 0.07 g/L/h and a 38% yield (mol/mol) in a fed-batch bioreactor. Here, the resulting strain with the deletion of *hexR, gntZ,* and *gacS* achieved 22.0 g/L at 0.21 g/L/h and a 35.6% yield (mol/mol) from glucose in similar conditions. These strategies enabled enhanced muconic acid production and may also improve production of other target molecules from glucose in *P. putida*.

1. Introduction

The range of renewable, biologically-produced fuels, chemicals, and materials has expanded significantly in response to the looming crisis of global climate change. Concurrently, the repertoire of microorganisms used for the generation of bioproducts has also grown. While model organisms such as *Saccharomyces cerevisiae* and *Escherichia coli* have invaluably advanced the nascent bioeconomy, a wealth of diversity can be found in organisms that exhibit beneficial phenotypes such as resistance to low pH, high flux to target or near-target products, and high stress tolerance to toxic substrates and products.

Of particular interest, *Pseudomonas putida* KT2440 has received

* Corresponding author.
** Corresponding author.
E-mail addresses: christopher.johnson@nrel.gov (C.W. Johnson), gregg.beckham@nrel.gov (G.T. Beckham).

https://doi.org/10.1016/j.ymben.2020.01.001
Received 6 October 2019; Received in revised form 1 January 2020; Accepted 4 January 2020
Available online 10 January 2020

significant attention as an important chassis for bioproduction (Nikel et al., 2016; Nikel and de Lorenzo, 2018). *P. putida* KT2440 is a Gram-negative, stress-tolerant, and genetically tractable soil bacterium with a rich diversity of metabolic pathways, enabling facile genetic engineering towards products of interest from multiple feedstocks (Aparicio et al., 2018; Cook et al., 2018; Johnson and Beckham, 2015 Johnson et al., 2019; Kim et al., 2000; Linger et al., 2014; Loeschcke and Thies, 2015; Mi et al., 2014; Nikel et al., 2016; Nikel and de Lorenzo, 2018, 2014; Vardon et al., 2015). For glucose consumption, *P. putida* KT2440 utilizes a combination of the Entner-Doudoroff, gluconeogenic Embden-Meyerhoff-Pernass, and the pentose phosphate pathways that together form the EDEMP cycle (Nikel et al., 2015). Use of the EDEMP cycle has been shown to provide an excess of NADPH reducing power, which may partially explain the exceptional stress resistance of this organism to a wide range of toxic molecules (Chavarría et al., 2013).

A particular target molecule that has been pursued for production in *P. putida* is *cis,cis*-muconic acid (referred to here as muconic acid or muconate). Muconic acid is considered a "bioprivileged" molecule, one that can be converted to multiple direct and functional replacements (Shanks and Keeling, 2017). In particular, it can be readily catalytically hydrogenated to adipic acid (Draths and Frost, 1994; Settle et al., 2019; Vardon et al., 2016, 2015), partially hydrogenated to 3-hexenedioic acid (Suastegui et al., 2016), catalytically converted to *trans,trans*-muconic acid (Carraher et al., 2017; Settle et al., 2018), and coupled with ethylene and dehydrogenated to form terephthalic acid (Lu et al., 2016). Muconic acid (both the *cis,cis*- and *trans,trans*-isomers) can also be used directly in performance-advantaged bioproducts such as high strength fiber-reinforced plastics or combined with plastics for upcycling reclaimed polyesters (Rorrer et al., 2016, 2017, 2019).

Multiple metabolic engineering studies have established biochemical routes to muconate from glucose and from lignin-derived aromatics (Becker et al., 2018; Draths and Frost, 1994; Johnson et al., 2016; 2019; Kohlstedt et al., 2018; Niu et al., 2002; Salvachúa et al., 2018; Sonoki et al., 2018; Vardon et al., 2015). Muconate can be produced from glucose by routing carbon into the shikimate pathway via condensation of erythrose-4-phosphate (E4P) and phosphoenolpyruvate (PEP) to form 3-deoxy-D-arabinoheptulosonate 7-phosphate (DAHP). From there, a series of native and heterologous enzymatic steps further metabolize DAHP to muconate (Fig. 1).

In *P. putida,* one factor potentially limiting muconate productivity from glucose is the preferential oxidation of glucose to gluconate and 2-ketogluconate. Substantially higher flux is directed through the periplasmic oxidation of glucose to gluconate and 2-ketogluconate than through direct glucose uptake and phosphorylation (Nikel et al., 2015; Kohlstedt and Wittmann, 2019). Significant 2-ketogluconate secretion and accumulation has been observed by our group and others when *P. putida* was cultivated in the presence of glucose (Borrero-De Acuña et al., 2014; Nijkamp et al., 2005). In our previously reported muconate-producing strain CJ442 (Table 1), 2-ketogluconate accumulation exceeded 40 g/L in a bioreactor (Johnson et al., 2019). This accumulation can be avoided by deleting the glucose dehydrogenase (encoded by *gcd*). While the *gcd* deletion introduces a slight growth defect in wild-type *P. putida* (del Castillo et al., 2007), deletion of *gcd* from engineered strain CJ442 generated a significant growth deficiency, with the new strain CJ522 showing a lag exceeding 120 h as well as slower muconate production (Johnson et al., 2019). This slow growth and production are major barriers to commercial viability.

The following work sought to improve the muconate production rate in strains lacking the 2-ketogluconate pathway. Adaptive laboratory evolution combined with biosensor-based high throughput screening, followed by whole genome sequencing suggested that the glucose metabolism is limiting in strains lacking the 2-ketogluconate pathway. We subsequently identified engineering targets to improve the muconate production rate, specifically by modulating regulation of glucose metabolism. Taken together, the findings presented in this work enable improved glucose conversion to muconate and provide new information regarding the regulatory landscape of glucose metabolism in *P. putida* KT2440.

2. Materials and methods

2.1. Plasmid construction

We used Phusion® High-Fidelity Polymerase (New England Biolabs) for all polymerase chain reactions. Gibson Assembly® Master Mix (New England Biolabs) or NEBuilder HiFi Assembly Master Mix (New England Biolabs) was used for plasmid construction followed by transformation into chemically competent NEB 5-α F'I^q *E. coli* (New England Biolabs) or electrocompetent *P. putida* KT2440. Transformants were selected on Lysogeny Broth (LB) agar plates containing 10 g/L tryptone, 5 g/L yeast extract, 5 g/L NaCl, and 15 g/L agar, supplemented with 50 μg/mL kanamycin (Kan_{50}) and grown overnight at 37°C or 30°C for *E. coli* or *P. putida*, respectively. Resulting constructs were confirmed by Sanger sequencing (GENEWIZ, Inc.). Detailed plasmid construction information is reported in the **Supplemental Information**.

2.2. Strain construction

Electrocompetent cells were prepared by inoculating *P. putida* strains from a glycerol stock into LB medium, and cultivating overnight with shaking at 225 rpm at 30°C. Electrocompetent cells were prepared by washing in 300 mM sucrose according to the method developed by (Choi et al., 2006). Transformations were performed by adding 200–500 ng of plasmid DNA to 60 μL of electrocompetent cells that were then electroporated using a Gene Pulser Xcell (Bio Rad) with recommended bacterial electroporation parameters for the cuvette size (0.1 or 0.2 cm). The cells were immediately resuspended in 800 μL of SOC outgrowth medium (New England Biolabs) and recovered for 2 h in a 1.5 mL microcentrifuge tube at 30°C and shaking at 225 rpm.

Gene replacements were performed as described in detail in our previous work by Johnson and Beckham (2015) using a selection (*nptII*, kanamycin), counterselection (*sacB,* sucrose) approach using the gene replacement backbone pK18sB (Jayakody et al., 2018). Correct gene replacements were diagnosed by colony PCR using MyTaq™ Red Mix (Bioline), with primers that anneal outside of the targeting homology arms. Colonies were patched on LB agar and LB Kan_{50} agar to ensure kanamycin sensitivity. Strains used in this study are described in Table 1.

2.3. Shake flask and microplate reader culture growth

Shake flask experiments were performed by inoculating seed cultures from glycerol stocks into 5 mL of LB medium, incubating overnight at 30°C and 225 rpm. Overnight cultures were then used to inoculate a second seed culture in LB medium starting at an optical density of 0.2 measured at 600 nm (OD_{600}) using a Beckman DU640 spectrophotometer (Beckman Coulter). The second seed cultures were incubated at 30°C at 225 rpm for 2–3 h until an OD_{600} of approximately 2 was reached. These seed cultures were centrifuged at 4500 rpm for 5 min, the pellets were resuspended in 1X M9 salts, and were used to inoculate the shake flasks containing modified M9 minimal media comprising 6.78 g/L Na_2HPO_4, 3 g/L KH_2PO_4, 0.5 g/L NaCl, 1 g/L NH_4Cl, 2 mM $MgSO_4$, 100 μM $CaCl_2$, 18 μM $FeSO_4$, and 25 mM or 30 mM glucose, as specified in text, to a starting OD_{600} of 0.1. Culture growth was monitored by periodic measurement of the OD_{600} along with collection of samples for metabolite analysis after passing samples through a 0.2 μm filter.

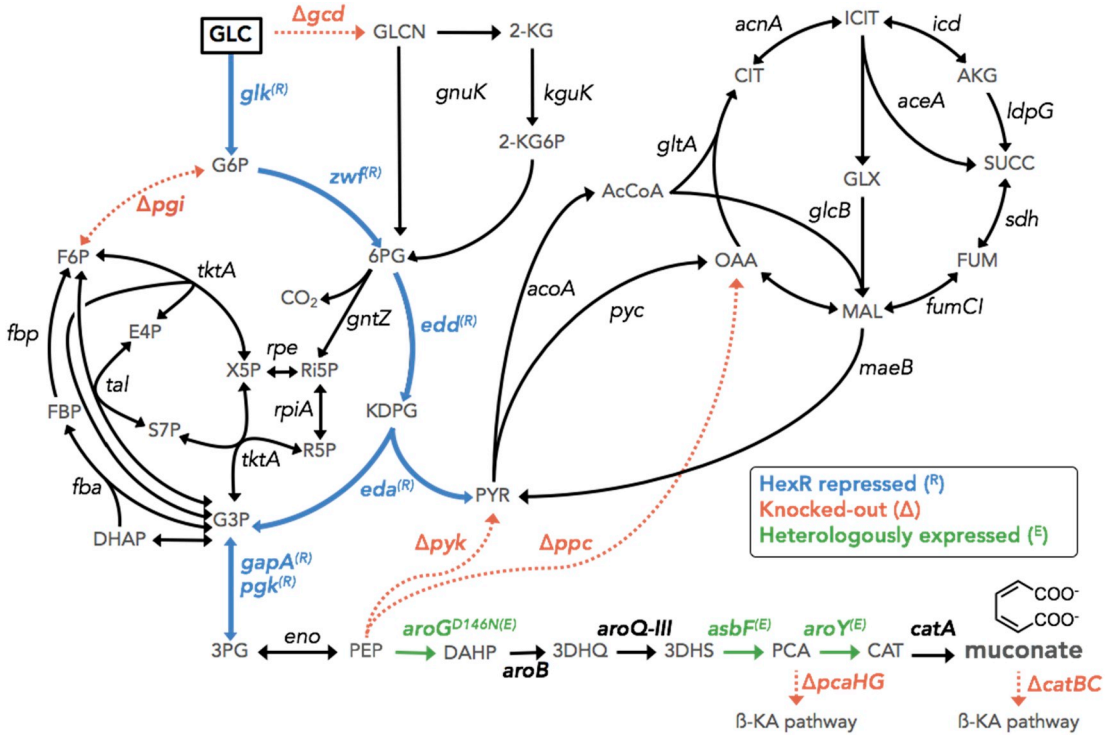

Fig. 1. Metabolic pathway for muconate production in engineered *P. putida* strain CJ522. Deleted genes are shown in orange; heterologous genes are shown in green with a superscript (*E*); genes repressed by HexR are shown in blue with a superscript (*R*). Phosphoenolpyruvate (PEP) is directed to muconate production via expression of a feedback resistant DAHP synthase (encoded by *aroG*-D146N derived from *E. coli*) followed by overexpression of a 3-dehydroshikimate (3-DHS) dehydratase (encoded by *asbF* derived from *Bacillus cereus* ATCC 14579), which generates protocatechuate (PCA) from 3-DHS. The strain maintains native genes expressing DAHP synthases and the 3DHS dehydratase (encoded by *quiC*). A protocatechuate decarboxylase (encoded by *aroY* derived from *Enterobacter cloacae* ATCC 13047) and the corresponding accessory protein that generates the prenylated flavin cofactor (encoded by *ecdB* derived from *Enterobacter cloacae* ATCC13047) are overexpressed to convert PCA to catechol (CAT). The native *catA* is overexpressed to ring-open catechol to *cis,cis*-muconate. The catabolic genes downstream of muconate, *catBC*, and the regulator *catR* are deleted. Competition for PEP is reduced by deletion of pyruvate kinase (encoded by *pykA* and *pykF*) and pyruvate carboxylase (encoded by *ppc*). Deletion of glucose-6-isomerase (encoded by *pgi-1* and *pgi-2*) interrupts the EDEMP cycle and directs flux to erythrose-4-phospate (E4P) and deletion of glucose dehydrogenase (encoded by *gcd*) eliminates the conversion of glucose to gluconate and 2-ketogluconate. Abbreviations are as follows: P: phosphate; GLC: glucose; GLCN: gluconate; 2-KG: 2-ketogluconate; 2-KG6P: 2-ketogluconate-6-P; G6P: glucose-6-P; 6PG: 6-phosphogluconate; KDPG: 2-keto-3-deoxy-6-phosphogluconate; G3P: glyceraldehyde-3-P; FBP: fructose-1,6-P_2; F6P: fructose-6-P; X5P: xylose-5-P; S7P: sedoheptulose-7-P; E4P: erythrose-4-P; R5P: ribose-5-P; Ri5P: ribulose-5-P; 3PG: glycerate-3-P; PEP: phosphoenolpyruvate; DHAP: dihydroxyacetone-P; DAHP: 3-deoxy-D-arabinoheptulosonate 7-phosphate; 3DHQ: 3-dehydroxyquinate; ICIT: isocitrate; CIT: citrate; AKG: alpha-ketoglutarate; SUCC: succinate; FUM: fumarate; MAL: malate; GLX:; OAA: oxaloacetate; AcCoA: acetyl-Coenzyme A; PYR: pyruvate.

2.4. Metabolite analysis

Prior work has quantified muconate using methods that are unable to discern its isomerization, which is known to occur spontaneously at pH < 7 (Carraher et al., 2017). The *cis,cis*- and *cis,trans*-muconate isomers exhibit different detector response factors, so if these isomers are not resolved, the resulting quantification is inaccurate. Muconate titers were therefore likely underestimated slightly in previous work. Here, a new method was developed to quantify *cis,cis*- and *cis,trans*-muconic acid isomers. Analysis of total muconic acid in this study was performed as outlined according to the procedure in NREL Laboratory Analytical Procedure (Black et al., 2019). An Agilent 1200 Series system (Agilent Technologies) equipped with a diode array detector (DAD) monitoring at 265 nm and a refractive index detector (RID) was used. Separation of *cis,cis*- and *cis,trans*-muconic acid isomers was achieved on a Luna C18(2) column 5 μm, 4.6 × 150 mm (Phenomenex) using an isocratic mobile phase of water/methanol (80/20) with 0.16% formic acid at a flow of 0.65 mL/min for a total run time of 15 min. The temperature of the column and RID were held constant at 45°C. Samples and standards were injected at a volume of 8 μL. Analytical standards of *cis,cis*- and *cis,trans*-muconic acid were prepared individually from a range of 0.5–1000 mg/L. Detector response for quantitation was based from calibration curves with an R^2 value ≥ 0.995.

Analysis of glucose was performed on an Agilent 1200 Series HPLC system (Agilent Technologies) equipped with an RID. Separation was achieved using a Shodex SP0810 sugar column 7 μm, 8 × 300 mm (Shodex) and isocratic flow of 0.6 mL/min mobile phase of HPLC grade water for a total run time of 42 min. The temperature of the column and RID were held constant at 85°C and 55°C, respectively. Each sample and standard were injected at a volume of 10 μL. Analytical standards were purchased from AbsoluteStandard and ranged from 0.5 to 36 g/L. A standard curve with a R^2 value ≥ 0.995 was employed for quantification. Deviation of the calibration verification standard (CVS) did not exceed 3%. Gluconate and 2-ketogluconate were analyzed according to previously published methods (Borrero-De Acuña et al., 2014).

2.5. Adaptive laboratory evolution

Serial passaging was performed in modified M9 minimal medium described above with 30 mM glucose as a sole carbon source and incubation at 30°C with shaking at 225 rpm. 1% (vol/vol) of the culture was transferred into fresh medium after growth was observed, which initially took up to 72 h of cultivation. The OD_{600} was measured at each passage to record the number of generations, calculated using the formula: number of generations = $\ln(OD_{final}/OD_{initial})/\ln(2)$. Performance of evolved strains was assayed by isolating clones and measuring growth on M9 with 30 mM glucose using a TECAN Infinite 200 microplate reader (TECAN US). 150 μL of medium inoculated to an

Table 1
Strains employed and generated in this study.

Strain	Genotype	Plasmid	References
CJ072	*P. putida* KT2440 Δ*pcaHG*	N/A	Jha et al. (2018)
CJ184	*P. putida* KT2440 Δ*catRBC*::Ptac:*catA* Δ*pcaHG*::Ptac:*aroY*:*ecdBD*	N/A	Johnson et al. (2016)
CJ442	*P. putida* KT2440 Δ*catRBC*::Ptac:*catA* Δ*pcaHG*::Ptac:*aroY*:*ecdB*:*asbF* Δ*pykA*::*aroG-D146N*:*aroY*:*ecdB*:*asbF* Δ*pykF* Δ*ppc* Δ*pgi-1* Δ*pgi-2*	N/A	Johnson et al. (2019)
CJ522	CJ442 Δ*gcd*	N/A	Johnson et al. (2019)
RJ12D	CJ184	pCatM	This study
RJ17A	CJ184	pCatM_lib	This study
RJ17O	CJ184	pCatM_C2	This study
RJ17P	CJ072	pCatM_C2	This study
GB032	CJ522 Δ*gltR1*	N/A	This study
GB038	CJ522-derived evolved population	N/A	This study
GB045	GB038 isolated clone #80	N/A	This study
GB052	GB038	pCatM_C2	This study
GB062	CJ522 Δ*hexR*	N/A	This study
GB099	CJ522 Δ*hexR* Δ*gltR1*	N/A	This study
GB209	GB062 Δ*gacS*	N/A	This study
GB210	CJ522 Δ*gacS*	N/A	This study
GB241	CJ522 Δ*gntZ*	N/A	This study
GB250	CJ522 Δ*gacS* Δ*gntZ*	N/A	This study
GB270	GB062 Δ*gntZ*	N/A	This study
GB271	GB062 Δ*gacS* Δ*gntZ*	N/A	This study
NN21	GB052 sorted clone 1	pCatM_C2	This study
NN23	GB052 sorted clone 9	pCatM_C2	This study
NN97	NN21, plasmid cured	N/A	This study
NN103	NN23, plasmid cured	N/A	This study
GB388	*P. putida* KT2440 Δ*benABC*	pCatM_C2	This study
GB391	*P. putida* KT2440 Δ*catA2* Δ*catBCA*	pCatM_C2	This study

OD_{600} of 0.1 was loaded into individual wells of a 96 well plate. Growth was monitored every 15 min, shaking with an amplitude of 4 mm at 30°C. Resulting OD_{600} measurements were normalized using a standard curve to correlate with the output from the Beckman DU640 spectrophotometer. Growth rates were calculated automatically by taking the natural log of the OD_{600} values measured by the TECAN and using a Python script to automatically calculate the maximum slope of 4 points during cultivation. Growth lag was calculated as the time required to enter stationary phase. Strains were preserved periodically as glycerol stocks at −80°C.

2.6. Biosensor mediated screening of evolved population

Detailed muconate sensor development information is described in the **Supplemental Information**. The evolved population was transformed with the muconate-responsive biosensor construct pCatM_C2 (according to the procedure in Section *2.2*), generating population GB052. For sorting, the GB052 population was revived from a glycerol stock by cultivation overnight in LB Kan_{50} liquid medium and further sub-cultured for 8 h. The culture was diluted to an OD_{600} of 0.01 in phosphate buffered saline (PBS) and analyzed and sorted on a BD FACSAria III flow cytometer and sorter (BD Biosciences) with standard settings for GFP fluorescence and with the cell population tightly gated for forward versus side scatter (FSC/SSC). A two-step method was used for sorting. In the first round, the top 5% of fluorescent cells were isolated by sorting followed by their recovery in LB Kan_{50} liquid medium overnight. In the second round, this culture subpopulation was sorted on the top 1% of fluorescent cells, and the isolates were recovered on LB Kan_{50} agar plates.

2.7. Plasmid curing for removal of muconate sensor plasmid from the production strains

The cell-sorted strains carrying the pCatM_C2 plasmid were cultivated in LB medium in the absence of antibiotic pressure for 7 days with sub-culturing 1% (v/v) into 25 mL LB every 24 h. After this period of sub-culturing, cells were diluted 1,000-fold in PBS and analyzed and sorted using a BD FACSAria III flow cytometer (BD Biosciences). Cells lacking GFP signal were isolated, and the sorted 'dark' population was plated on LB agar plates. Dark colonies were further selected using the Illumatool Lighting System (Lightools Research) with 488 nm excitation wavelength and viewed through 515 nm long pass filter. Several dark colonies were patched on LB agar and LB agar Kan_{50} to confirm kanamycin sensitivity. Clones that were sensitive to kanamycin were preserved for further analysis. PCR was additionally used to confirm the absence of the sensor plasmid.

2.8. Genome resequencing library preparation

Genomic DNA for sequencing was isolated from LB broth overnight cultures using the ZR Fungal/Bacterial DNA miniprep kit (Zymo Research). The quality of genomic DNA was analyzed by gel electrophoresis. An Illumina Nextera XT library (Illumina) was prepared as described in the manufacturer's protocols, stopping after library validation. Briefly, the sample was fragmented, barcodes were appended, and the sample was amplified for 12 cycles. The library was then cleaned using AMPure XP beads (Beckman Coulter). The final library was validated on an Agilent Bioanalyzer (Agilent Technologies) using a DNA7500 chip and concentration was determined on a Qubit (Life Technologies) with the broad range double stranded DNA assay (Life Technologies). The library was prepared for sequencing following the manufacturer's protocols. The library was denatured with 0.2 N NaOH and diluted to the final sequencing concentration. The library was then loaded into the sequencing cassette (v3) and a paired end (2 × 301) run was completed on an Illumina MiSeq Instrument. Comparison of the parent and evolved isolate genome sequences was performed using the Geneious software package version 10.2.3 (Biomatters Ltd) (Kearse et al., 2012).

2.9. Transcriptomics

Cells pelleted from 15 mL of M9 minimal medium were flash frozen and stored at −80°C. Cells were resuspended in TRIzol (ThermoFisher-Invitrogen) and processed according to the manufacturer's protocol. The samples were then purified on an RNeasy column (Qiagen) with on-column DNase digestion. RNA was eluted off the column in 35 μL RNase free H_2O (Qiagen). The RNA concentration was quantified using a Nanodrop 1000 (ThermoScientific) and RNA quality was verified by obtaining RNA Integrity Numbers (RIN) using an RNA 6000 Nanochip on an Agilent 2100 Bioanalyzer (Agilent).

Ribosomal RNA was depleted using a RiboZero rRNA Removal Kit for bacteria (Illumina). The depleted sample was purified on an RNA Clean & Concentrator-5 (Zymo Research), and then the depleted material was quantified using a Nanodrop 1000 and visualized on an Agilent 2100 Bioanalyzer instrument with an RNA 6000 Nanochip (Agilent). RNA depleted of ribosomal RNA was used as input material to synthesize cDNA libraries using a ScriptSeq v2 RNA-Seq Library Preparation Kit (Illumina) and TruSeq compatible barcodes. Pooled barcoded libraries were sequenced in one direction for 75 bases (SE75) on an Illumina NextSeq500 (Illumina) and de-multiplexed as a sequencing service provided by Vanderbilt *2.9* (VUMC VANTAGE Vanderbilt University Medical Center Technologies for Advanced Genomics). Raw sequencing reads were trimmed with the Geneious trim function using an error probability limit of 0.04 and remaining default parameters. Trimmed reads were aligned to the *P. putida* KT440 genome (accession #NZ_LT799039), containing the known genome

modifications in CJ522 using the Geneious RNA mapper with medium sensitivity. Differential expression analysis was computed using the DESeq2 (Love et al., 2014) method within Geneious using default parameters. Adjustment of P-values for multiple hypothesis testing was performed within DESeq2 using the method of Benjamini and Hochberg (1995).

2.10. Bioreactor cultivations

To evaluate the performance of muconate-producing strains in bioreactors, a fed-batch cultivation mode was used. The strains were revived from glycerol stocks in 125 mL baffled flasks containing 25 mL LB and incubated at 30°C and 220 rpm for 16 h. Cells were then inoculated into 1 L baffled flasks with 200 mL LB at an initial OD_{600} of 0.2 and incubated in the same conditions for approximately 3.5 h. When the OD_{600} reached 2, 10% (v/v) of that culture was transferred to 0.5 L bioreactors (BioStat-Q Plus, Sartorius Stedim Biotech). The bioreactor medium contained modified M9 (13.56 g/L Na_2HPO_4, 6 g/L KH_2PO_4, 1 g/L NaCl, 2 mM $MgSO_4$, 100 μM $CaCl_2$, and 18 μM $FeSO_4$) plus 25 g/L glucose and 5 g/L $(NH_4)_2SO_4$. Bioreactors were controlled at pH 7 with 4 N NH_4OH, at 30°C, and air was sparged at 1 vvm. The initial agitation speed was 350 rpm. When the dissolved oxygen (DO) reached a value of 30%, it was automatically controlled at that level by agitation. When the glucose concentration decreased to approximately 5 g/L in the batch phase, the feeding was activated to maintain glucose levels between 5 and 15 g/L. The feeding medium consisted of 500 g/L glucose and 100 g/L $(NH_4)_2SO_4$ and was pH adjusted (pH 7) with NaOH. Samples were taken periodically to evaluate bacterial growth and to analyze glucose and metabolites. The cultivations ended at 104 h, when glucose utilization rates decreased considerably in most of the strains. Calculations of performance metrics are described in the **Supplemental Information**.

3. Results

3.1. Adaptive laboratory evolution for improved cell growth

To improve the growth of *P. putida* muconate-producing strain CJ522 on glucose as a sole carbon source, adaptive laboratory evolution was performed. Prior work demonstrated the metabolic preference for the gluconate pathway (Nikel et al., 2015). Eliminating *gcd* thus reroutes this carbon flux, likely explaining the growth defect exhibited by this strain. We hypothesized that adaptive laboratory evolution could identify solutions to overcome this defect. Serial transfers (1% v/v) were performed after 24 h, or until visible growth occurred (Fig. 2A). Initially, 72 h were required to observe growth. Breakout growth occurred after approximately 45 generations, when growth became visible after only overnight cultivation. The resulting population was preserved as GB038 (Fig. 2A).

Isolates derived from the GB038 population were screened for growth using a microplate reader. The parent strains CJ442 and CJ522 were included in the comparison of the heterogeneous evolved population (GB038) and isolated clones (Fig. 2A, shown in light blue). The dramatic growth defect caused by *gcd* deletion in CJ522 was apparent compared to the progenitor strain CJ442 maintaining *gcd*, consistent with Johnson et al. (2019). A wide variety of growth phenotypes was observed among the evolved isolates, with most isolates exhibiting improved growth compared to the heterogeneous evolved population GB038 and the unevolved parent strain CJ522 (Fig. 2A). Many evolved clones exhibit increased maximum specific growth rates (μ), compared to CJ522 in addition to reduced lag (Fig. 2B). Of the evolved isolates, GB045 demonstrated substantially improved growth, reaching a higher μ faster than CJ442 (Fig. 2B). Based on these results, muconate production by GB045 was next evaluated in a shake flask experiment.

A new analytical method (**Materials and Methods**, *Section 2.4*) was used in this work that can quantify *cis,cis* and *cis,trans*-muconic acid (Black et al., 2019). Using this new method, the percentage of *cis,trans*-muconate was observed to reach ~10–15% in shake flask cultivations and ~5–8% in pH-controlled bioreactors. Muconate production of GB045 peaked nearly 60 h earlier than the parent strain CJ522 (Fig. 3A, B). Although GB045 produced muconate more quickly, the final muconate titer was significantly lower ($P < 0.0001$). While our analytical method focused on specifically quantifying muconic acid and glucose as the key metabolites, no other appreciable peaks were observed that would indicate substantial production of co-products.

3.2. Muconate-responsive biosensor development for product-based screening

While most isolates from the GB038 population grew faster than CJ522, these evolved isolates did not necessarily make more muconate, as evidenced by strain GB045 (Fig. 3B). An alternative approach would be to use high throughput screening based on muconate production to isolate strains with both improved growth and muconate production. A fluorescence-activated cell sorting (FACS)-based, high-throughput assay would enable the isolation of cells based on muconate production,

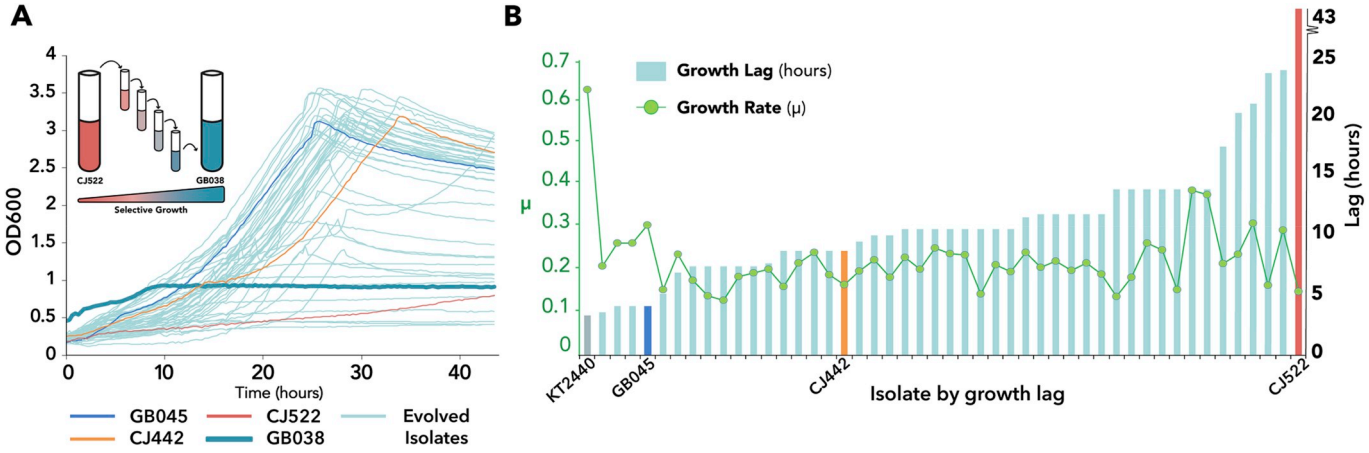

Fig. 2. Characterization of evolved clones. Deletion of *gcd* in CJ442 generated CJ522. Both strains are shown for comparison. (**A**) Serial passaging of strain CJ522 was performed using 1% (vol/vol) of culture to inoculate fresh M9 minimal medium containing 30 mM glucose (top left inset). Population GB038 demonstrated improved growth. Growth of evolved population GB038 is compared on a microplate reader to clones isolated from the population. Strain GB045 is a clonal isolate derived from population GB038 and was selected for further analysis. (**B**) Growth rate of clonal isolates plotted by the time in hours (lag) required to reach the maximum specific growth rate (μ).

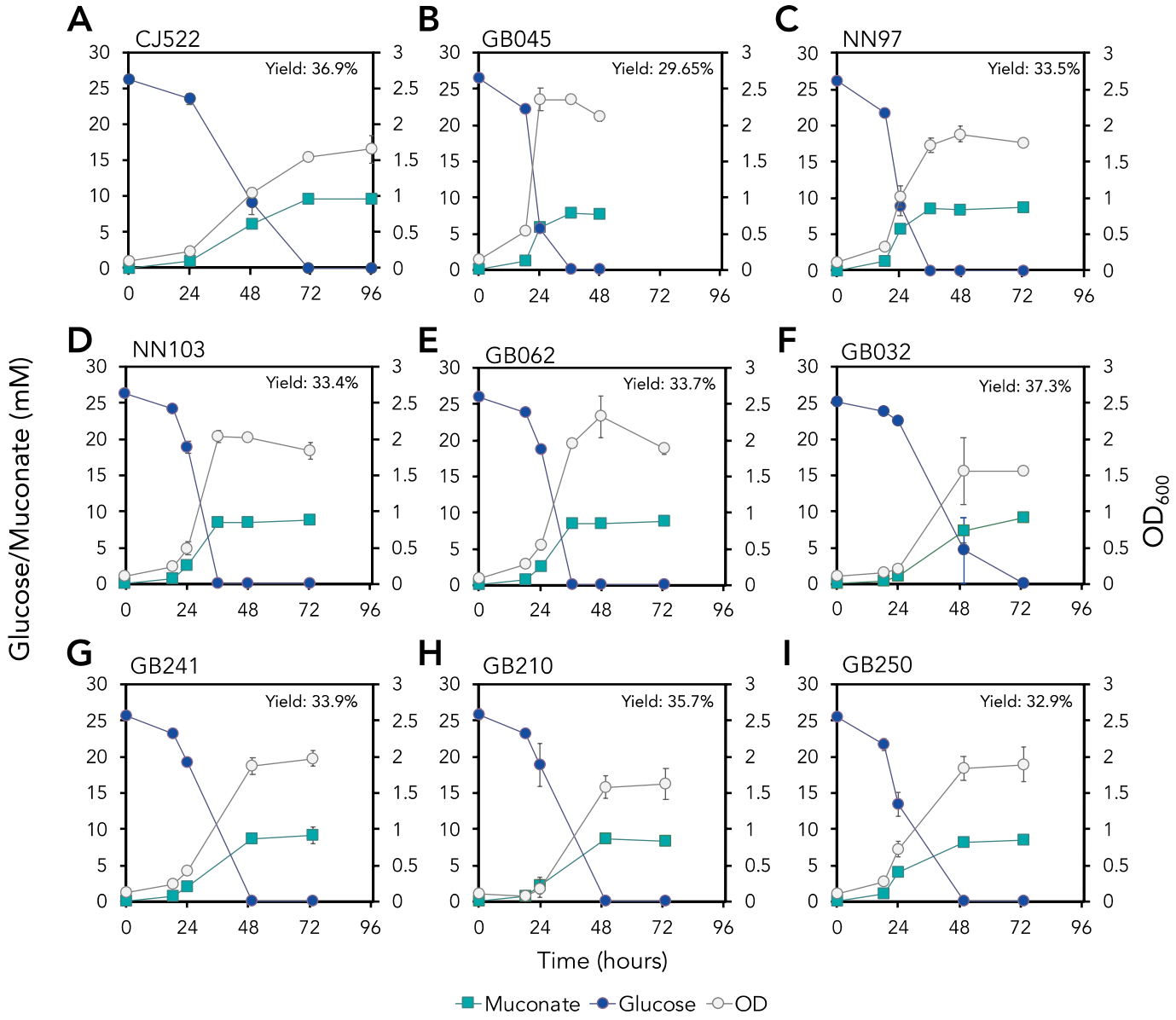

Fig. 3. Shake flask characterization of engineered and evolved strains. (**A**) Performance of CJ522, (**B**) GB045 (CJ522 evolved isolate 80), (**C**) NN97 (sorted isolate 1), (**D**) NN103 (sorted isolate 9), (**E**) GB062 (CJ522 Δ*hexR*), (**F**) GB032 (CJ522 Δ*gltR1*), (**G**) GB241 (CJ522 Δ*gntZ*), (**H**) GB210 (CJ522 Δ*gacS*), (**I**) GB250 (CJ522 Δ*gacS* Δ*gntZ*). Each value represents the average of biological triplicates, with error bars representing the standard deviation of the replicates. Glucose and muconate concentrations measured by HPLC are shown, in addition to the OD_{600} at each timepoint. Yield was calculated at the timepoint where maximum muconate was accumulated.

but first requires a functional muconate-responsive biosensor.

3.2.1. Sensor-reporter construct for muconate detection

Given its prevalence as a key intermediate in the ß-ketoadipate pathway, several organisms have evolved muconate-responsive regulators (Harwood and Parales, 1996). Two well-studied transcription factors that respond to muconate are CatM and BenM from *Acinetobacter baylyi* ADP1 (Tropel and van der Meer, 2004). While previous muconate sensors have been established in *E. coli* (Rogers and Church, 2016) and *S. cerevisiae* (Skjoedt et al., 2016), both were developed using BenM, where cross-reactivity with benzoate via a secondary binding site is well-documented (Ezezika et al., 2007). CatM was therefore selected to be developed into a muconate sensor in *P. putida*. The sensor, pCatM, was constructed such that transcription of superfolder GFP (*sfgfp*) (Pédelacq et al., 2006) was under the control of the *catM-catB* intergenic promoter region (referred to as P_{catB}), consisting of three CatM binding sites (Ezezika et al., 2006) (Figs. 4A and S1).

P. putida KT2440 cannot grow on muconic acid as a sole carbon source, suggesting that muconic acid transport is poor, so a precursor that can be imported and metabolized to muconate was used to characterize the sensor. A strain engineered to efficiently convert the precursors PCA, benzoate, and catechol to muconate (CJ184, Johnson et al., 2016) was used to characterize the sensor pCatM. Unfortunately, muconate produced from PCA did not induce expression of GFP (Figs. 4B and S1A, pCatM), indicating additional sensor optimization was necessary. The ribosome binding site (RBS) was replaced by an optimal sequence, which has previously been shown to improve sensor dynamic range (Jha et al., 2014). The promoter and operator sites were also diversified to improve the dynamic range (Fig. S1B). A plasmid library (pCatM_lib) including > 65,000 RBS, promoter, and operator combinations was constructed and transformed into strain CJ184 (Johnson et al., 2016), generating library RJ17A. RJ17A was then

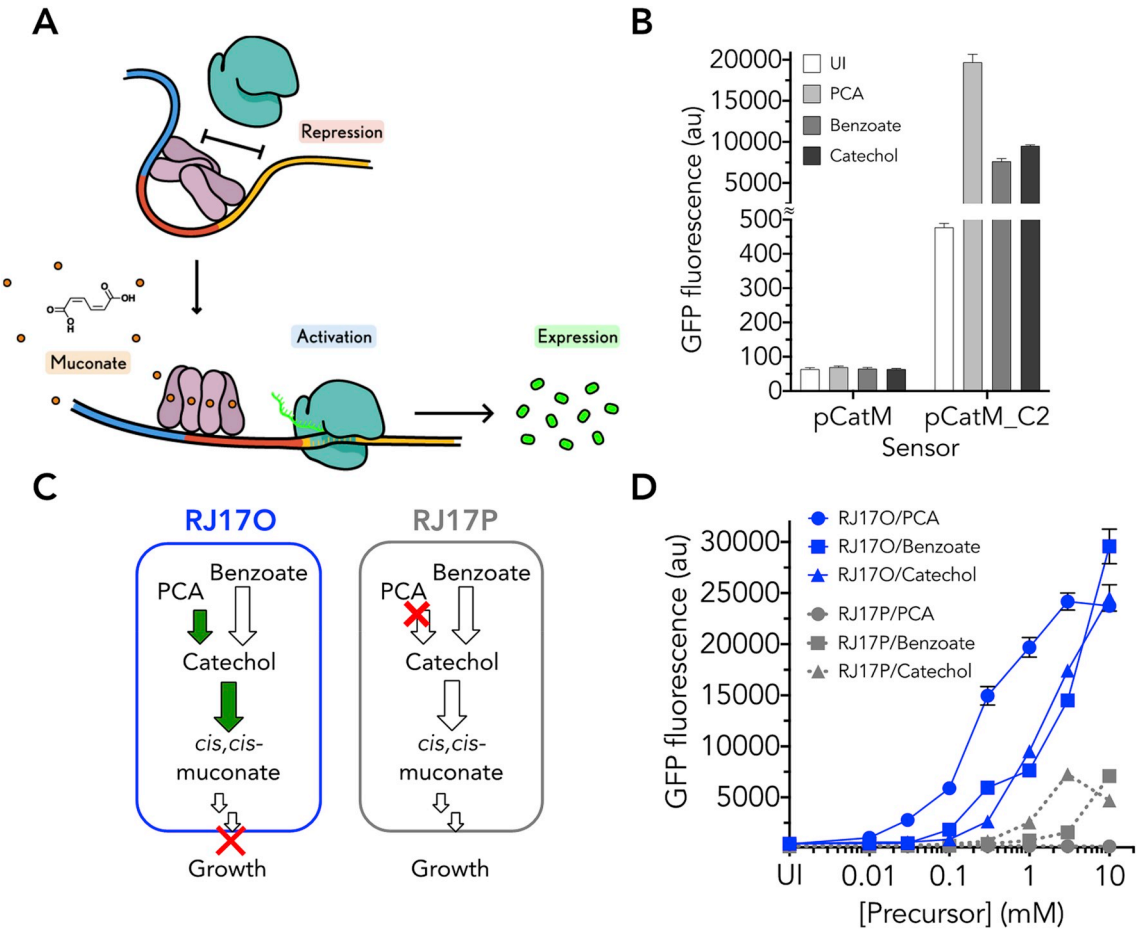

Fig. 4. Fluorescence-activated cell sorting of an evolved population carrying the CatM-based biosensor construct. (**A**) Illustration of CatM activation of gene expression in the presence of muconate. (**B**) GFP fluorescence based on activation of the muconate biosensor construct in a *P. putida* strain that accumulates muconate (CJ184, Johnson et al., 2016). pCatM uses the native promoter sequence from *A. baylyi* sp. ADP1, while pCatM_C2 contains an optimized promoter sequence. Uninduced (UI) indicates cells grown in the absence of any precursor molecule, or cells were grown in the presence of 1 mM PCA, benzoate, or catechol. (**C**) Depiction of muconate production and catabolism in the two strains used for testing the muconate biosensor in (D). RJ17O is strain CJ184 (Johnson et al., 2016) containing pCatM_C2, and RJ17P is CJ072 (Jha et al., 2018) containing pCatM_C2. Green arrows depict overexpressed genes. Genes absent for a particular step are marked with a red cross. (**D**) Performance of strains RJ17O and RJ17P with various concentrations of PCA, benzoate, and catechol using Accuri C6 (BD Biosciences) flow cytometer. Each data point represents the mean and standard deviation of three biological replicates. Note: 10 mM catechol in the media showed a dark brown coloration and potential toxicity effects resulted in larger cellular size and granularity as shown by higher forward and side scatter (FSC, SSC) values compared to other concentrations and precursors.

screened using FACS in the presence of PCA and other muconate precursors (Fig. S2). Clones were isolated for further characterization and construct pCatM_C2 was identified as the top muconate-responsive variant, exhibiting low background fluorescence and high dynamic range (Figs. 4B and S2C).

Unlike the initial sensor pCatM, pCatM_C2 introduced into strain CJ184 (strain RJ17O) showed a clear dose-dependent response to intracellular muconate generated by metabolism of PCA, benzoate, and catechol (Fig. 4B, D). In order to test the specificity of the sensor, pCatM_C2 was transformed into CJ072 (Jha et al., 2018), generating strain RJ17P (Fig. 4C). When RJ17P was exposed to benzoate and catechol, a dose-dependent fluorescent response was observed due to an intact catechol branch of the β-ketoadipate pathway (Fig. 4C and D). Since the catabolic genes of muconate are intact in RJ17P, the intracellular muconate concentration is expected to be lower than in RJ17O, due to the metabolism of muconate for cellular growth. Consistent with this, the sensor response was substantially lower in RJ17P than in RJ17O (Fig. 4D). Cross reactivity of the sensor to benzoate, catechol, and PCA was also evaluated, none of which activated the sensor (Fig. S3). The direct correlation between muconate concentration and fluorescence was determined by measuring the fluorescence response and muconate concentration in strains fed with a range of muconate precursor concentrations (Fig. S4). Together, these data demonstrate that the optimized construct pCatM_C2 is a suitable sensor of intracellular muconate in *P. putida*.

3.2.2. FACS isolation of muconate-producing cells

This new muconate-responsive biosensor was deployed to isolate clones with improved muconate production from the evolved population GB038. This population was transformed with the pCatM_C2 biosensor and the resulting population, now designated GB052, was analyzed for muconate-induced GFP fluorescence by flow cytometry. Multiple GFP populations were observed, confirming muconate production heterogeneity within the evolved population. The cells with the highest 5% GFP signal were collected, followed by regrowth and sorting of cells with the top 1% of GFP fluorescence in the second round (Fig. S5). From here, two clones were isolated and named NN21 and NN23.

3.2.3. Shake flask characterization of sorted clones

The muconate production of these sorted clones was examined next. Since the isolated clones carried the biosensor plasmid, the clones were first cured of the plasmid to eliminate any associated metabolic burden,

Table 2
Mutations identified in evolved isolates.

Gene	Category	Affected Strains
glyA-II	substitution	GB045
cyoB	substitution	GB045
fleQ	deletion	GB045
lapA	insertion	NN103
edd promoter	substitution	NN97
gacS	insertion	GB045 and NN97
PP_3142:PP_3194	deletion	GB045
PP_4031:PP_4058, including *gntZ*, *zwf-2*, and *spp*	deletion	NN103

generating strains NN97 and NN103, from NN21 and NN23 respectively (Table 1). A shake flask cultivation was performed, and both strains demonstrated improved growth compared to strain CJ522. NN97 and NN103 reached maximum muconate titers after 36 h of cultivation, nearly 60 h faster than the parent strain CJ522 (Fig. 3C, D). Compared to the clone selected on the basis of growth alone, GB045, these clones produced muconate at a similar rate and ultimately accumulated significantly higher titers ($P < 0.05$). These data demonstrate that strain screening using a muconate-responsive biosensor within an evolved population enables the isolation of individual clones with improved muconate production.

3.3. Whole genome sequencing (WGS) of evolved clones

To identify mutations underlying improved performance, the genomes of the evolved clones were sequenced. Strain GB045 contains mutations in five loci relative to the parent strain CJ522 (Table 2, Table S4). Mutations in PP_4373 (*fleQ*) and PP_1650 (*gacS*) likely disrupt the function of these two global regulators. FleQ is required for flagellar function in many Pseudomonads, including *P. putida* KT2440 (Blanco-Romero et al., 2018), and is itself downregulated during stationary phase in many Pseudomonads by the GacS/GacA two-component system (Kim et al., 2014). Disruption of GacS was also observed to reduce lag time and improve growth in *Pseudomonas* sp. PCL1171 (van den Broek et al., 2005), suggesting the *gacS* disruption plays a role in the observed improved growth phenotype. Notably, a large deletion was identified in the GB045 genome, spanning a region of 122,413 base pairs, including multiple transcriptional regulators and the benzoate degradation operon (*benA-benK*) (Table 2).

Sequencing of the clones isolated by FACS revealed additional mutations. Isolate NN97 contains a substitution mutation in the *edd* (PP_1010) and *gap-1* (PP_1009) promoter region. Normally, transcription of these two genes and downstream operons, as well as the remainder of the Entner-Doudoroff pathway, is tightly regulated by the repressor HexR. The mutation does not appear to be located in either of the two known HexR operators in this region bound by HexR; therefore the σ^{70} promoter prediction software, BPROM (Solovyev, V.; Salamov, 2011) was used to analyze the sequence for new promoters. The BPROM prediction indicated that the mutation may generate a new −10 sequence upstream of the *edd* operon that could increase expression of *edd*, *glk*, *gltR2*, and the sensor histidine kinase partner of GltR2 (encoded by gene PP_1013). In addition to the promoter mutation, NN97 also contains a transposon insertion into *gacS* identical to that observed in GB045, again suggesting that this mutation is beneficial for growth (Table 2). The second sorted strain NN103 contains a deletion of approximately 35,000 base pairs, distinct from the deleted region in GB045. The deleted region includes an operon (PP_4043 to PP_4041) encoding three proteins involved in sugar metabolism: 6-phosphogluconate dehydrogenase (*gntZ*), glucose 6-phosphate 1-dehydrogenase (*zwf-2*), and sugar phosphate phosphohydrolase (*spp*) (Table 2). NN103 also contains two transposon insertions into *lapA* (PP_0168), a large adhesion protein critical for biofilm formation in *P. putida* (Hinsa et al., 2003).

3.4. Rational engineering for enhanced muconate production in P. putida KT2440

Genome resequencing data suggested that regulators of glucose metabolism may serve as promising targets for strain engineering. One such regulator, HexR, is a transcription factor that represses expression of genes involved in the glycolytic portion of the EDEMP pathway in the absence of 2-keto-3-deoxy-6-P-gluconate (KDPG) (Fig. 1). Another transcriptional regulator, GltR, has been characterized as an activator of glucose uptake and the *gtsABCD* operon in response to allosteric regulation by 2-ketogluconate (del Castillo et al., 2008) and is itself regulated by HexR. Thus, we next explored the effect of deleting these regulators on glucose metabolism from the unevolved strain CJ522. *P. putida* KT2440 contains two paralogs of GltR, with prior reports characterizing GltR2 (Daddaoua et al., 2014; del Castillo et al., 2008). Deletion of *gltR2* was not successful, indicating essentiality in the CJ522 background, even though this gene was readily deleted in *P. putida* KT2440 (data not shown). The *gltR1* gene was deleted from CJ522 to generate strain GB032 and the *hexR* gene was deleted to generate GB062.

In shake flask experiments, GB062 grew more rapidly on glucose, as it reached its maximum muconate titer of 8.5 ± 0.16 mM after only 36 h of cultivation, compared to 96 h required for CJ522 to reach its maximum titer (Fig. 3A, E). Deletion of *gltR1* from CJ522 (strain GB032) only marginally improved the growth and muconate production rate compared to CJ522 (Fig. 3F). Deletion of *hexR* and *gltR1* in combination was evaluated to determine whether an additive or synergistic effect may occur. Interestingly, the strain lacking both regulators, strain GB099, performed similarly to GB062 (Figs. S6B and C), suggesting that if GltR1 plays a role, HexR maintains epistatic dominance over GltR1.

Mutations in *gntZ* and *gacS* identified in the sorted evolved clones suggested that deletion of these genes may additionally enhance growth and muconate production. Deletion of *gntZ* in CJ522 (strain GB241) increased the muconate production rate, such that the maximum muconate titer was reached at 72 h, compared to CJ522 which required 96 h (Fig. 3G). Similarly, deletion of *gacS* (strain GB210) improved muconic acid productivity where the maxiumum titer was reached after only approximately 50 h (Fig. 3H). Deletion of both *gntZ* and *gacS* in CJ522 (strain GB250) only slightly improved strain performance when evaluated in a shake flask (Fig. 3I). These deletions were next tested in the top performing engineered strain, GB062 (CJ522 Δ*hexR*). Deletion of *gacS* (strain GB209), *gntZ* (strain GB270), or both *gntZ* and *gacS* (strain GB271) from strain GB062 did not noticeably improve muconic acid production or growth compared to GB062, when evaluated in a shake flask (Figs. S6D–F).

3.5. Transcriptomic analysis of engineered strains

In order to better understand how deletion of *hexR* affects glucose metabolism, transcriptomics experiments were performed comparing wild-type *P. putida* KT2440, CJ522, and GB062 at mid-log phase of growth (OD_{600} ~0.7), cultivated on glucose as a sole carbon source. The majority of variation in the expression of the 5,555 detected transcripts was driven by genotype, with wild-type separating strongly from both engineered strains by principal component analysis (Fig. S7). A pairwise comparison of CJ522 and GB062 identified 81 genes with a $\log_2$ fold-change of > 1 and $p < 0.005$ (higher abundance in GB062) and 116 with a $\log_2$ fold-change of < -1 and $p < 0.005$ (higher abundance in CJ522) (Fig. 5).

Several genes related to alginate production (*mucA, mucB, alg* suite) were down-regulated in GB062. Alginate is an anionic polysaccharide composed of ß-(1,4)-linked *n*-mannuronic and L-guluronic acids. Pseudomonad alginate biosynthesis has been studied in response to environmental stressors (Damron and Yu, 2011; Deretic et al., 1987). Control of *zwf* expression is linked to alginate production in *P. aeruginosa* (Silo-Suh et al., 2005), but an association between alginate and HexR in *P. putida* is unclear. Several transcription factors up-regulated in GB062 may be interesting targets for future study (Figs. 5B and S5).

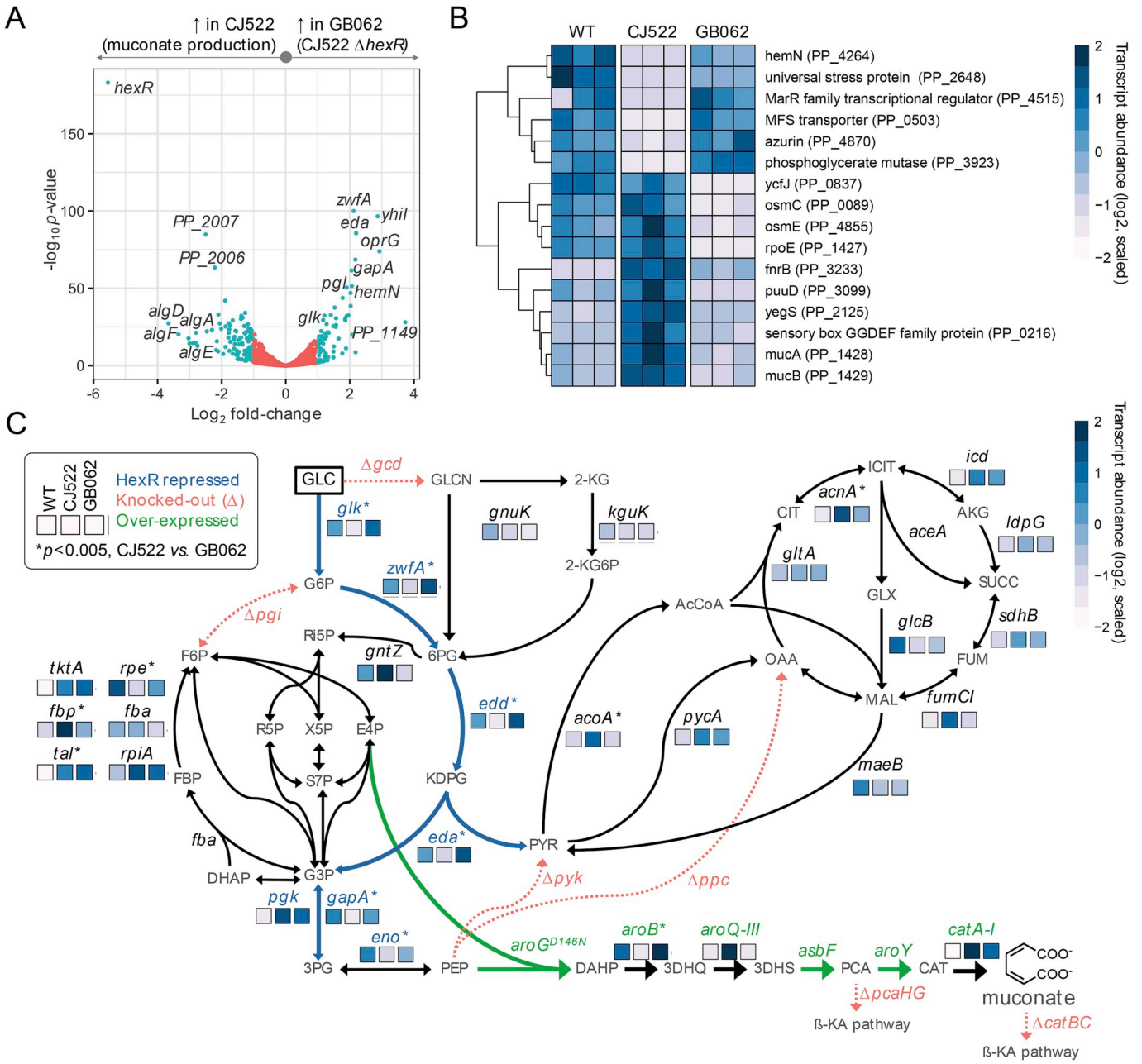

Fig. 5. HexR deletion in GB062 relieves transcriptional repression of central carbon pathways. (**A**) Volcano plot of pairwise comparison between GB062 and CJ522 on glucose ($p < 0.005$, Log_2 fold-change $> |1|$). (**B**) Select hits from (A) plotted as a clustered heat-map with individual values from biological triplicates. Additional heat maps for redundant transcripts are shown in Fig. S8 and denoted by ‡ (**C**) Metabolic pathway toward muconate production with heat-mapped transcript abundance overlaid. The average of biological triplicates is presented. Abbreviations are as follows: P: phosphate; GLC: glucose; GLCN: gluconate; 2-KG: 2-ketogluconate; 2-KG6P: 2-ketogluconate-6-P; G6P: glucose-6-P; 6PG: 6-phosphogluconate; KDPG: 2-keto-3-deoxy-6-phosphogluconate; G3P: glyceraldehyde-3-P; FBP: fructose-1,6-P_2; F6P: fructose-6-P; X5P: xylose-5-P; S7P: sedoheptulose-7-P; E4P: erythrose-4-P; R5P: ribose-5-P; Ri5P: ribulose-5-P; 3PG: glycerate-3-P; PEP: phosphoenolpyruvate; DHAP: dihydroxyacetone-P; ICIT: isocitrate; CIT: citrate; AKG: alpha-ketoglutarate; SUCC: succinate; FUM: fumarate; MAL: malate; GLX:; OAA: oxaloacetate; AcCoA: acetyl-Coenzyme A; PYR: pyruvate.

As expected, the *hexR* deletion in GB062 increased expression of *glk, zwf, edd, eda,* and *gapA* (Fig. 5C, Table S5) (del Castillo et al., 2008). *Rpe, tal, eno,* and *aroB* were also significantly up-regulated in GB062 wheras *acoA* and *acnA* were significantly down-regulated (Fig. 5C., Table S5). Together, the transcriptomic data suggest that deletion of *hexR* in this strain restores expression of HexR-repressed genes in the pentose phosphate pathway and Entner-Doudoroff pathway and may also contribute to dysregulation of stress responses such as alginate production..

3.6. Bioreactor cultivations to assess strain performance

To more deeply characterize the top performing strains, pH-controlled fed-batch bioreactors were run on strains GB062 (CJ522 Δ*hexR*), GB271 (CJ522 Δ*hexR,* Δ*gntZ*, Δ*gacS*), NN97 (CJ522 evolved isolate 1), and NN103 (CJ522 evolved isolate 9). The cultivations were maintained for 104 h (Figs. S9–10), after which glucose utilization rates decreased considerably in most of the strains, likely due to product toxicity (Salvachúa et al., 2018). The primary bioreactor results (titers, yields, and rates) are presented in Fig. 6. GB062 produced muconate to

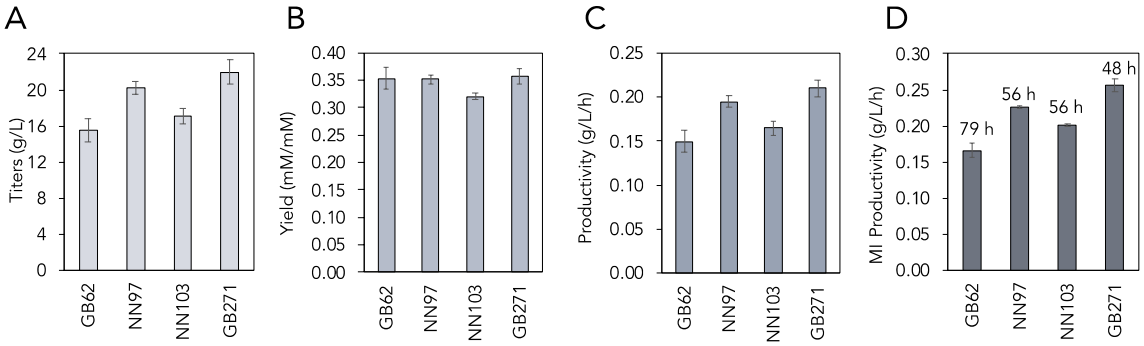

Fig. 6. Strain performance in bioreactors. (**A**) Muconate titers (g/L), (**B**) metabolic yields (mol/mol), (**C**) overall productivities (g/L/h), and maximum instantaneous (MI) productivities (g/L/h) from fed-batch cultivations by a subset of engineered muconate-producing strains. The numbers on the top of the bars in graph (**D**) indicate the time (h) at which the maximum productivity was observed. Results show the average of biological duplicates and error bars the absolute difference between replicates. Detailed bioreactor profiles are shown in Figs. S9 and S10.

a concentration of 15.6 g/L. NN97 outperformed GB062, reaching a titer of 20.3 g/L (Fig. 6A).

Interestingly, although deletion of *gntZ* and *gacS* did not noticeably improve performance of GB062 in a shake flask experiment, GB271 reached the highest titer (22.0 g/L). The yields were similar between strains GB062, NN97, and GB271 (~ 35%) (Fig. 6B). The four strains tested demonstrated productivity improvements compared to the parent strain CJ522 (0.07 g/L/h) in similar batch-fed bioreactor cultivations (Johnson et al., 2019). The overall and maximum instantaneous productivities in NN97 were 0.195 and 0.226 g/L/h, respectively while in GB062, they were 0.15 and 0.17 g/L/h, respectively (Fig. 6C–D). Strain GB271 showed additionally improved performance, reaching an overall and maximum productivity of 0.21 and 0.256 g/L/h, respectively.

These results demonstrate that the combination of *hexR, gacS,* and *gntZ* deletion enable the best performance observed, critically overcoming the productivity barrier that this work sought to improve. This dataset represents a substantial improvement from titers and productivities obtained by CJ442 and CJ522 in bioreactors using similar cultivation conditions in previous work by our group (Johnson et al., 2019). Titers and overall rates were 7 g/L and 0.07 g/L/h (at 104 h) in CJ522 and 9 g/L and 0.08 g/L/h (at 115 h) in CJ442 (Johnson et al., 2019). The latter strain also accumulated 46 g/L of 2-ketogluconate which resulted in lower muconate yields (23%) (Johnson et al., 2019). In this engineered strain background, muconate yields are metabolically constrained by the availability of only one PEP per glucose molecule, generating a maximum theoretical yield of 50% (mol/mol) (Johnson et al., 2019). In this work, we were able to maintain comparable yields to CJ522, approaching the theoretical maximum, while improving the productivity by 3-fold.

Overall, this work presents, to our knowledge, the highest muconate titers and productivities from glucose by engineered *P. putida* reported to date. Further bioreactor and strain development remain necessary to continue increasing titers, yields, and productivities as well as product tolerance, and these efforts are currently underway.

4. Discussion and conclusions

In this work, we explored several approaches to overcome a growth defect caused by deletion of the glucose dehydrogenase in *P. putida* KT2440 engineered to produce muconate from glucose. Without this deletion, substantial 2-ketogluconate accumulates, reducing muconate yield and productivity (Johnson et al., 2019). We employed three methods to improve strain performance: evolution, biosensor-enabled screening, and rational engineering. In this work, the ability to screen for clones based on muconate production dramatically affected the performance of resulting strains. When evolved strains were isolated based on growth alone, the resulting clones demonstrated improved growth, but the muconate production suffered. The development of a muconate-responsive biosensor for use in *P. putida* therefore enabled the isolation of evolved clones based on the product of interest, muconic acid. This biosensor enabled isolation of clones with dramatically improved muconate production, in addition to improved growth, demonstrating the utility of screening in conjunction with adaptive laboratory evolution. Between these two approaches, mutations observed in the isolated clones were able to direct targeted engineering efforts. Mutations in the *edd* promoter directed us to delete *hexR,* in addition to mutations suggesting the involvement of GntZ and GacS and strain performance. Deletion of these three genes resulted in improved strain growth and muconic acid production.

We hypothesize that *hexR* deletion represents a generalizable target to improve glucose metabolism in strains lacking *gcd* due to the unique carbon catabolite repression employed by *P. putida* KT2440. In contrast with many other Gram-negative bacteria that prefer hexose sugar carbon sources, *P. putida* naturally prefers organic acids and amino acids to glucose (Rojo, 2010). Further, when *P. putida* is grown on glucose, the majority of the glucose is not directly assimilated, but is preferentially routed through the periplasmic gluconate and 2-ketogluconate pathways, and secreted in the presence of abundant glucose (Nikel et al., 2015). Accordingly, it was expected that relieving repression of glucose metabolism, mediated by HexR, would improve strain performance, particularly when the gluconate pathway is blocked. Indeed, eliminating this regulator allowed much more rapid glucose metabolism to growth and muconate. The *hexR* gene was previously deleted with the intent to improve flux to E4P, but in a strain that maintained the glucose dehydrogenase (Yu et al., 2016). In that context, deletion of *hexR* improved *p*-hydroxybenzoic acid production from glucose. The deletion of *hexR* here in the context of a *gcd* deletion may have generated two distinct benefits: allowing for the activation of genes for glucose metabolism and increasing carbon flux from glucose through the EDEMP cycle to E4P, one of the critical substrates in the first committed reaction of the shikimate pathway (Draths and Frost, 1994).

Beyond improving performance, we sought to develop more mechanistic understanding of the phenotype observed after *hexR* deletion in a strain unable to produce 2-ketogluconate. We compared the two otherwise isogenic engineered strains with and without *hexR*: CJ522 and GB062. The transcriptomics data provide a comprehensive snapshot of the wide-ranging effects that this single gene deletion introduces, including 197 differentially expressed transcripts. Differential expression of genes in the context of *hexR* deletion in KT2440 was previously studied, but only 8 transcripts with significant differential expression were identified (del Castillo et al., 2008). As our assay investigated differential expression in an engineered strain background, the increased number of reads may provide additional information on how the deletion of *hexR* may improve performance of engineered strains.

Deletion of *gntZ* likely eliminated a competing pathway for 6PG consumption, increasing flux to KDPG, which would allosterically release HexR repression of many of the key initial glucose metabolic genes (Fig. 1). In that way, deletion of *gntZ* was able to improve the performance of CJ522, but in a background where *hexR* is already eliminated, the effect was negligible, as was reflected in our shake flask data (Fig. 3).

Our prior work modeled the minimum selling price (MSP) of muconic acid based on metabolic yield and productivity (Johnson et al., 2019). Previously, strain CJ522 produced muconate at ~40% yield (mol/mol) and 0.07 g/L/h. This performance corresponds with a MSP above $4/kg. Here, the best performing strain, GB271, produced muconate at a similar yield as CJ522. The increase in productivity to 0.21 g/L/h would enable a reduction in the MSP of more than $1/kg (Johnson et al., 2019). Improving these metrics represents an important step towards commercial viability of microbial muconate production from glucose.

As interest in *P. putida* as a chassis organism grows, improved glucose utilization will be a critical parameter for biological conversion. Furthermore, substantial accumulation of 2-ketogluconate in a bioreactor is untenable, especially considering the sensitivity of *P. putida* to acidic conditions. The results of this work have identified solutions to eliminate 2-ketogluconate accumulation by *P. putida* while maintaining its ability to effectively utilize glucose. Our work improved the ability of engineered *P. putida* to grow on glucose and convert that substrate to muconate. This lays the foundation for future *P. putida* metabolic engineering efforts to convert sugars into chemicals.

Notes

The authors declare competing financial interest. Modified biosensors and biocatalysts and methods of use are subjects of patent applications by Los Alamos National Laboratory. GJB, DS, JRE, AMG, GLP, GTB, CWJ, TD, NN, and RKJ have submitted patent applications on engineered strains related to this work.

Acknowledgements

This work was authored in part by Alliance for Sustainable Energy, LLC, the manager and operator of the National Renewable Energy Laboratory for the U.S. Department of Energy (DOE) under Contract No. DE-AC36-08GO28308.

This work has also been authored in part by employees of Triad National Security, LLC, operator of the Los Alamos National Laboratory under Contract No.89233218CNA000001 with the U.S. Department of Energy. This work was also partially authored Oak Ridge National Laboratory, which is managed by UT-Battelle, LLC, for the U.S. DOE under contract DE-AC05-00OR22725. Funding was provided by the U.S. Department of Energy Office of Energy Efficiency and Renewable Energy Bioenergy Technologies Office (BETO) for the Agile BioFoundry (to TD (Contract NL0032182), AMG, and GTB). We thank Jay Fitzgerald at DOE and members of the Agile BioFoundry for helpful discussions. We thank Rita Clare for designing and preparing Figs. 2 and 4A. We thank Babetta Marrone and Laboratory Directed Research and Development grant from Los Alamos National Laboratory (project 20160656ER) for supporting preliminary work on sensor development. We thank Jay Huenemann for plasmid construction assistance. Joshua Vermaas wrote the Python script to calculate the specific growth rate.

Appendix A. Supplementary data

Supplementary data to this article can be found online at https://doi.org/10.1016/j.ymben.2020.01.001.

References

Aparicio, T., de Lorenzo, V., Martínez-García, E., 2018. CRISPR/Cas9-Based counterselection boosts recombineering efficiency in Pseudomonas putida. Biotechnol. J. 13, 1700161. https://doi.org/10.1002/biot.201700161.

Becker, J., Kuhl, M., Kohlstedt, M., Starck, S., Wittmann, C., 2018. Metabolic engineering of Corynebacterium glutamicum for the production of cis, cis-muconic acid from lignin. Microb. Cell Factories 17, 115. https://doi.org/10.1186/s12934-018-0963-2.

Benjamini, Y., Hochberg, Y., 1995. Controlling the false discovery rate: a practical and powerful approach to multiple testing. J. R. Stat. Soc. Ser. B 57, 289–300. https://doi.org/10.2307/2346101.

Black, B.A., Michener, W.E., Payne, C.E., Beckham, G.T., 2019. Determination of Cis,cis- and Cis,trans-Muconic Acid from Biological Conversion: Laboratory Analytical Procedure (LAP). Issue Date: August 30, 2019. https://www.nrel.gov/docs/fy19osti/74473.pdf.

Blanco-Romero, E., Redondo-Nieto, M., Martínez-Granero, F., Garrido-Sanz, D., Ramos-González, M.I., Martín, M., Rivilla, R., 2018. Genome-wide analysis of the FleQ direct regulon in Pseudomonas fluorescens F113 and Pseudomonas putida KT2440. Sci. Rep. 8, 13145. https://doi.org/10.1038/s41598-018-31371-z.

Borrero-De Acuña, J.M., Bielecka, A., Häussler, S., Schobert, M., Jahn, M., Wittmann, C., Jahn, D., Poblete-Castro, I., 2014. Production of Medium Chain Length Polyhydroxyalkanoate in Metabolic Flux Optimized Pseudomonas Putida. https://doi.org/10.1186/1475-2859-13-88.

van den Broek, Daan, Chin-A-Woeng, Thomas F.C., Bloemberg, G.V., L, B.J.J., 2005. Role of RpoS and MutS in phase variation of Pseudomonas sp. PCL1171. Microbiology 151, 1403–1408. https://doi.org/10.1099/mic.0.27777-0.

Carraher, J.M., Pfennig, T., Rao, R.G., Shanks, B.H., Tessonnier, J.-P., 2017. cis,cis-Muconic acid isomerization and catalytic conversion to biobased cyclic-C_6 -1,4-diacid monomers. Green Chem. 19, 3042–3050. https://doi.org/10.1039/C7GC00658F.

del Castillo, T., Ramos, J.L., Rodríguez-Herva, J.J., Fuhrer, T., Sauer, U., Duque, E., 2007. Convergent peripheral pathways catalyze initial glucose catabolism in Pseudomonas putida: genomic and flux analysis. J. Bacteriol. 189, 5142–5152. https://doi.org/10.1128/JB.00203-07.

del Castillo, T., Duque, E., Ramos, J.L., 2008. A set of activators and repressors control peripheral glucose pathways in Pseudomonas putida to yield a common central intermediate. J. Bacteriol. 190, 2331–2339. https://doi.org/10.1128/JB.01726-07.

Chavarría, M., Nikel, P.I., Pérez-Pantoja, D., de Lorenzo, V., 2013. The Entner-Doudoroff pathway empowers *Pseudomonas putida* KT2440 with a high tolerance to oxidative stress. Environ. Microbiol. 15, 1772–1785. https://doi.org/10.1111/1462-2920.12069.

Choi, K.-H., Kumar, A., Schweizer, H.P., 2006. A 10-min method for preparation of highly electrocompetent Pseudomonas aeruginosa cells: application for DNA fragment transfer between chromosomes and plasmid transformation. J. Microbiol. Methods 64, 391–397. https://doi.org/10.1016/j.mimet.2005.06.001.

Cook, T.B., Rand, J.M., Nurani, W., Courtney, D.K., Liu, S.A., Pfleger, B.F., 2018. Genetic tools for reliable gene expression and recombineering in Pseudomonas putida. J. Ind. Microbiol. Biotechnol. 1–11. https://doi.org/10.1007/s10295-017-2001-5.

Daddaoua, A., Molina-Santiago, C., de la Torre, J., Krell, T., Ramos, J.-L., 2014. GtrS and GltR form a two-component system: the central role of 2-ketogluconate in the expression of exotoxin A and glucose catabolic enzymes in Pseudomonas aeruginosa. Nucleic Acids Res. 42, 7654–7663. https://doi.org/10.1093/nar/gku496.

Damron, F.H., Yu, H.D., 2011. Pseudomonas aeruginosa MucD regulates the alginate pathway through activation of MucA degradation via MucP proteolytic activity. J. Bacteriol. 193, 286–291. https://doi.org/10.1128/JB.01132-10.

Deretic, V., Gill, J.F., Chakrabarty, A.M., 1987. Alginate biosynthesis: a model system for gene regulation and function in Pseudomonas. Nat. Biotechnol. 5, 469–477. https://doi.org/10.1038/nbt0587-469.

Draths, K.M., Frost, J.W., 1994. Environmentally compatible synthesis of adipic acid from D-glucose. J. Am. Chem. Soc. 116, 399–400. https://doi.org/10.1021/ja00080a057.

Ezezika, O.C., Collier-Hyams, L.S., Dale, H.A., Burk, A.C., Neidle, E.L., 2006. CatM regulation of the benABCDE operon: functional divergence of two LysR-type paralogs in Acinetobacter baylyi ADP1. Appl. Environ. Microbiol. 72, 1749–1758. https://doi.org/10.1128/AEM.72.3.1749-1758.2006.

Ezezika, O.C., Haddad, S., Clark, T.J., Neidle, E.L., Momany, C., 2007. Distinct Effector-binding Sites Enable Synergistic Transcriptional Activation by BenM, a LysR-type Regulator. J. Mol. Biol. 367, 616–629. https://doi.org/10.1016/j.jmb.2006.09.090.

Harwood, C.S., Parales, R.E., 1996. The β-KETOADIPATE pathway and the biology OF self-identity. Annu. Rev. Microbiol. 50, 553–590. https://doi.org/10.1146/annurev.micro.50.1.553.

Hinsa, S.M., Espinosa-Urgel, M., Ramos, J.L., O'Toole, G.A., 2003. Transition from reversible to irreversible attachment during biofilm formation by Pseudomonas fluorescens WCS365 requires an ABC transporter and a large secreted protein. Mol. Microbiol. 49, 905–918.

Jayakody, L.N., Johnson, C.W., Whitham, J.M., Giannone, R.J., Black, B.A., Cleveland, N.S., Klingeman, D.M., Michener, W.E., Olstad, J.L., Vardon, D.R., Brown, R.C., Brown, S.D., Hettich, R.L., Guss, A.M., Beckham, G.T., 2018. Thermochemical wastewater valorization *via* enhanced microbial toxicity tolerance. Energy Environ. Sci. 11, 1625–1638. https://doi.org/10.1039/C8EE00460A.

Jha, R.K., Kern, T.L., Fox, D.T., Strauss, C.E.M., 2014. Engineering an *Acinetobacter* regulon for biosensing and high-throughput enzyme screening in *E. coli* via flow cytometry. Nucleic Acids Res. 42, 8150–8160. https://doi.org/10.1093/nar/gku444.

Jha, R.K., Bingen, J.M., Johnson, C.W., Kern, T.L., Khanna, P., Trettel, D.S., Strauss, C.E.M., Beckham, G.T., Dale, T., 2018. A protocatechuate biosensor for Pseudomonas putida KT2440 via promoter and protein evolution. Metab. Eng. Commun. 6, 33–38.

https://doi.org/10.1016/j.meteno.2018.03.001.
Johnson, C.W., Beckham, G.T., 2015. Aromatic catabolic pathway selection for optimal production of pyruvate and lactate from lignin. Metab. Eng. 28, 240–247. https://doi.org/10.1016/j.ymben.2015.01.005.
Johnson, C.W., Salvachúa, D., Khanna, P., Smith, H., Peterson, D.J., Beckham, G.T., 2016. Enhancing muconic acid production from glucose and lignin-derived aromatic compounds via increased protocatechuate decarboxylase activity. Metab. Eng. Commun. 3, 111–119. https://doi.org/10.1016/j.meteno.2016.04.002.
Johnson, C.W., Salvachú, D., Rorrer, N.A., Bomble, Y.J., Guss, A.M., Beckham, G.T., Black, B.A., Vardon, D.R., St John, P.C., Cleveland, N.S., Dominick, G., Elmore, J.R., Grundl, N., Khanna, P., Martinez, C.R., Michener, W.E., Peterson, D.J., Ramirez, K.J., Singh, P., VanderWall, T.A., Nolan Wilson, A., Yi, X., Biddy, M.J., 2019. Innovative chemicals and materials from bacterial aromatic catabolic pathways. Joule. https://doi.org/10.1016/j.joule.2019.05.011.
Kearse, M., Moir, R., Wilson, A., Stones-Havas, S., Cheung, M., Sturrock, S., Buxton, S., Cooper, A., Markowitz, S., Duran, C., Thierer, T., Ashton, B., Meintjes, P., Drummond, A., 2012. Geneious Basic: an integrated and extendable desktop software platform for the organization and analysis of sequence data. Bioinformatics 28, 1647–1649. https://doi.org/10.1093/bioinformatics/bts199.
Kim, D.Y., Kim, Y.B., Rhee, Y.H., 2000. Evaluation of various carbon substrates for the biosynthesis of polyhydroxyalkanoates bearing functional groups by Pseudomonas putida. Int. J. Biol. Macromol. 28, 23–29.
Kim, J.S., Kim, Y.H., Anderson, A.J., Kim, Y.C., 2014. The sensor kinase GacS negatively regulates flagellar formation and motility in a biocontrol bacterium, Pseudomonas chlororaphis O6. Plant Pathol. J. 30, 215–219. https://doi.org/10.5423/PPJ.NT.11.2013.0109.
J.Kohlstedt, M., Starck, S., Barton, N., Stolzenberger, J., Selzer, M., Mehlmann, K., Schneider, R., Pleissner, D., Rinkel, J., Dickschat, J.S., Venus, J., van Duuren, B.J.H., Wittmann, C., 2018. From lignin to nylon: cascaded chemical and biochemical conversion using metabolically engineered Pseudomonas putida. Metab. Eng. 47, 279–293. https://doi.org/10.1016/J.YMBEN.2018.03.003.
Kohlstedt, M., Wittmann, C., 2019. GC-MS-based 13 C metabolic flux analysis resolves the parallel and cyclic glucose metabolism of Pseudomonas putida KT2440 and Pseudomonas aeruginosa PAO1. Metab. Eng. 54, 35–53. https://doi.org/10.1016/j.ymben.2019.01.008.
Linger, J.G., Vardon, D.R., Guarnieri, M.T., Karp, E.M., Hunsinger, G.B., Franden, M.A., Johnson, C.W., Chupka, G., Strathmann, T.J., Pienkos, P.T., Beckham, G.T., 2014. Lignin valorization through integrated biological funneling and chemical catalysis. Proc. Natl. Acad. Sci. U.S.A. 111, 12013–12018. https://doi.org/10.1073/pnas.1410657111.
Loeschcke, A., Thies, S., 2015. Pseudomonas putida—a versatile host for the production of natural products. Appl. Microbiol. Biotechnol. 99, 6197–6214. https://doi.org/10.1007/s00253-015-6745-4.
Love, M.I., Huber, W., Anders, S., 2014. Moderated estimation of fold change and dispersion for RNA-seq data with DESeq2. Genome Biol. 15, 550. https://doi.org/10.1186/s13059-014-0550-8.
Lu, R., Lu, F., Chen, J., Yu, W., Huang, Q., Zhang, J., Xu, J., 2016. Production of diethyl terephthalate from biomass-derived muconic acid. Angew. Chem. 128, 257–261. https://doi.org/10.1002/ange.201509149.
Mi, J., Becher, D., Lubuta, P., Dany, S., Tusch, K., Schewe, H., Buchhaupt, M., Schrader, J., 2014. De novo production of the monoterpenoid geranic acid by metabolically engineered Pseudomonas putida. Microb. Cell Factories 13, 170. https://doi.org/10.1186/s12934-014-0170-8.
Nijkamp, K., van Luijk, N., de Bont, J.A.M., Wery, J., 2005. The solvent-tolerant Pseudomonas putida S12 as host for the production of cinnamic acid from glucose. Appl. Microbiol. Biotechnol. 69, 170–177. https://doi.org/10.1007/s00253-005-1973-7.
Nikel, P.I., de Lorenzo, V., 2014. Robustness of Pseudomonas putida KT2440 as a host for ethanol biosynthesis. N. Biotechnol. 31, 562–571. https://doi.org/10.1016/j.nbt.2014.02.006.
Nikel, P.I., de Lorenzo, V., 2018. Pseudomonas putida as a functional chassis for industrial biocatalysis: from native biochemistry to trans-metabolism. Metab. Eng. 50, 142–155. https://doi.org/10.1016/J.YMBEN.2018.05.005.
Nikel, P.I., Chavarría, M., Fuhrer, T., Sauer, U., de Lorenzo, V., 2015. Pseudomonas putida KT2440 strain metabolizes glucose through a cycle formed by enzymes of the entner-doudoroff, embden-meyerhof-parnas, and pentose phosphate pathways. J. Biol. Chem. 290, 25920–25932. https://doi.org/10.1074/jbc.M115.687749.
Nikel, P.I., Chavarría, M., Danchin, A., de Lorenzo, V., 2016. From dirt to industrial applications: Pseudomonas putida as a Synthetic Biology chassis for hosting harsh biochemical reactions. Curr. Opin. Chem. Biol. 34, 20–29. https://doi.org/10.1016/J.CBPA.2016.05.011.
Niu, W., Draths, K.M., Frost, J.W., 2002. Benzene-free synthesis of adipic acid. Biotechnol. Prog. 18, 201–211. https://doi.org/10.1021/bp010179x.
Pédelacq, J.-D., Cabantous, S., Tran, T., Terwilliger, T.C., Waldo, G.S., 2006. Engineering and characterization of a superfolder green fluorescent protein. Nat. Biotechnol. 24, 79–88. https://doi.org/10.1038/nbt1172.
Rogers, J.K., Church, G.M., 2016. Genetically encoded sensors enable real-time observation of metabolite production. Proc. Natl. Acad. Sci. U.S.A. 113, 2388–2393. https://doi.org/10.1073/pnas.1600375113.
Rojo, F., 2010. Carbon catabolite repression in *Pseudomonas* : optimizing metabolic versatility and interactions with the environment. FEMS Microbiol. Rev. 34, 658–684. https://doi.org/10.1111/j.1574-6976.2010.00218.x.
Rorrer, N.A., Dorgan, J.R., Vardon, D.R., Martinez, C.R., Yang, Y., Beckham, G.T., 2016. Renewable unsaturated polyesters from muconic acid. ACS Sustain. Chem. Eng. 4, 6867–6876. https://doi.org/10.1021/acssuschemeng.6b01820.
Rorrer, N.A., Vardon, D.R., Dorgan, J.R., Gjersing, E.J., Beckham, G.T., 2017. Biomass-derived monomers for performance-differentiated fiber reinforced polymer composites. Green Chem. 19, 2812–2825. https://doi.org/10.1039/C7GC00320J.
Rorrer, N.A., Nicholson, S., Carpenter, A., Biddy, M.J., Grundl, N.J., Beckham, G.T., 2019. Combining reclaimed PET with bio-based monomers enables plastics upcycling. Joule 3, 1006–1027. https://doi.org/10.1016/j.joule.2019.01.018.
Salvachúa, D., Johnson, C.W., Singer, C.A., Rohrer, H., Peterson, D.J., Black, B.A., Knapp, A., Beckham, G.T., 2018. Bioprocess development for muconic acid production from aromatic compounds and lignin. Green Chem. 20, 5007–5019. https://doi.org/10.1039/C8GC02519C.
Settle, A.E., Berstis, L., Zhang, S., Rorrer, N.A., Hu, H., Richards, R.M., Beckham, G.T., Crowley, M.F., Vardon, D.R., 2018. Iodine-catalyzed isomerization of dimethyl muconate. ChemSusChem 11, 1768–1780. https://doi.org/10.1002/cssc.201800606.
Settle, A.E., Cleveland, N.S., Farberow, C.A., Conklin, D.R., Huo, X., Dameron, A.A., Tracy, R.W., Sarkar, R., Kautz, E.J., Devaraj, A., Ramasamy, K.K., Watson, M.J., York, A.M., Richards, R.M., Unocic, K.A., Beckham, G.T., Griffin, M.B., Hurst, K.E., Tan, E.C.D., Christensen, S.T., Vardon, D.R., 2019. Enhanced catalyst durability for bio-based adipic acid production by atomic layer deposition. Joule 3 (9), 2219–2240. https://doi.org/10.1016/J.JOULE.2019.06.022.
Silo-Suh, L., Suh, S.-J., Phibbs, P.V., Ohman, D.E., 2005. Adaptations of < em > Pseudomonas aeruginosa < /em > to the cystic fibrosis lung environment can include deregulation of < em > zwf < /em > , encoding glucose-6-phosphate dehydrogenase. J. Bacteriol. 187, 7561–7568. https://doi.org/10.1128/JB.187.22.7561-7568.2005.
Shanks, B.H., Keeling, P.L., 2017. Bioprivileged molecules: creating value from biomass. Green Chem. 19, 3177–3185. https://doi.org/10.1039/C7GC00296C.
Skjoedt, M.L., Snoek, T., Kildegaard, K.R., Arsovska, D., Eichenberger, M., Goedecke, T.J., Rajkumar, A.S., Zhang, J., Kristensen, M., Lehka, B.J., Siedler, S., Borodina, I., Jensen, M.K., Keasling, J.D., 2016. Engineering prokaryotic transcriptional activators as metabolite biosensors in yeast. Nat. Chem. Biol. 12, 951–958. https://doi.org/10.1038/nchembio.2177.
Solovyev, V., Salamov, A., 2011. Automatic annotation of microbial genomes and metagenomic sequences. In: Metagenomics and its Applications in Agriculture, Biomedicine and Environmental Studies, pp. 61–78.
Sonoki, T., Takahashi, K., Sugita, H., Hatamura, M., Azuma, Y., Sato, T., Suzuki, S., Kamimura, N., Masai, E., 2018. Glucose-free *cis* , *cis* -muconic acid production via new metabolic designs corresponding to the heterogeneity of lignin. ACS Sustain. Chem. Eng. 6, 1256–1264. https://doi.org/10.1021/acssuschemeng.7b03597.
Suastegui, M., Matthiesen, J.E., Carraher, J.M., Hernandez, N., Rodriguez Quiroz, N., Okerlund, A., Cochran, E.W., Shao, Z., Tessonnier, J.-P., 2016. Combining metabolic engineering and electrocatalysis: application to the production of polyamides from sugar. Angew. Chem. Int. Ed. 55, 2368–2373. https://doi.org/10.1002/anie.201509653.
Tropel, D., van der Meer, J.R., 2004. Bacterial transcriptional regulators for degradation pathways of aromatic compounds. Microbiol. Mol. Biol. Rev. 68, 474–500. https://doi.org/10.1128/MMBR.68.3.474-500.2004.
Vardon, D.R., Franden, M.A., Johnson, C.W., Karp, E.M., Guarnieri, M.T., Linger, J.G., Salm, M.J., Strathmann, T.J., Beckham, G.T., 2015. Adipic acid production from lignin. Energy Environ. Sci. 8, 617–628. https://doi.org/10.1039/c4ee03230f.
Vardon, D.R., Rorrer, N.A., Salvachúa, D., Settle, A.E., Johnson, C.W., Menart, M.J., Cleveland, N.S., Ciesielski, P.N., Steirer, K.X., Dorgan, J.R., Beckham, G.T., 2016. cis,cis-Muconic acid: separation and catalysis to bio-adipic acid for nylon-6,6 polymerization. Green Chem. 18. https://doi.org/10.1039/c5gc02844b.
Yu, S., Plan, M.R., Winter, G., Krömer, J.O., 2016. Metabolic engineering of Pseudomonas putida KT2440 for the production of para-hydroxy benzoic acid. Front. Bioeng. Biotechnol. 4, 90. https://doi.org/10.3389/fbioe.2016.00090.